Normalized unitary synaptic signaling of the hippocampus and entorhinal cortex

Keivan Moradi
George Mason University   https://orcid.org/0000-0002-0778-9855

Zainab Aldarraji
George Mason University

Megha Luthra
George Mason University

Grey Madison
George Mason University

Giorgio A. Ascoli (✉ ascoli@gmu.edu)
George Mason University

Research Article

Abstract

Limited experimental yield, heterogeneous recordings conditions, and ambiguous neuronal identification have so far prevented the systematic characterization of synaptic signals for all connections of any neural system. Introducing a novel strategy to overcome these challenges, we report the first comprehensive synaptic quantification among all known neuron types of the hippocampal-entorhinal network. First, we reconstructed > 2,600 synaptic traces from ~ 1,200 publications into a unified model of synaptic dynamics. We then trained a deep learning architecture with the resulting parameters, each annotated with detailed metadata. The model learned to predict the synaptic properties of all 3,120 circuit connections in arbitrary conditions with accuracy approaching the intrinsic experimental variability. Analysis of normalized data revealed that synaptic signals are controlled by few latent variables associated with specific molecular markers and interrelating conductance, kinetics, and short-term plasticity. We freely release the tools and full dataset of unitary synaptic values in 32 covariate settings via Hippocampome.org.

Introduction

Understanding neuronal communication is key to decode brain function. Synapses mediate the transmission from the axon of a (sender) neuron to the dendrite or perisomatic area of a (receiver) neuron. An electrical signal is thus recordable from the postsynaptic cell upon activation of the presynaptic cell. Different synapses produce distinct signals ultimately orchestrating behavior and cognition[1]. Plastic changes in synaptic signaling subserve adaptive processes underlying memory. Identifying aberrant synaptic dynamics is crucial to the elucidation of the pathophysiology of diseases such as schizophrenia and depression[2, 3]. Yet, the synaptic physiology of most neuronal connections remains poorly understood.

The summed synaptic activity of multiple contacts connecting two neurons is a *unitary* signal. Unitary synaptic signals are typically measured by paired recording[4], also allowing for post-hoc identification of both presynaptic and postsynaptic neuronal types. Unfortunately, paired recordings are based on a blind search method with a low success rate in finding connected pairs. Accordingly, sample sizes for this method are typically small. Collating recordings from different studies may increase statistical power if they can be mapped to a common framework. Since neuronal connections require the anatomical co-location of a presynaptic axon and a postsynaptic dendrite (or soma), synapses could be classified based on the morphological patterns of the corresponding neurons[5]. The knowledge base Hippocampome.org recognizes 122 neuron types and 3,120 potential connections in the rodent hippocampus and entorhinal cortex[6, 7].

To coalesce data from the hippocampal formation, we mined approximately 1,200 publications, annotated more than 2,600 synaptic electrophysiology traces or values, extracted the signal measurements (synaptometrics), and mapped the data to the neuron types and potential connections of Hippocampome.org[8]. However, the data are in various formats, requiring unification into a common

formalism. This can be achieved using a phenomenological description of synaptic dynamics[9]. In such an approach, synaptic amplitude is defined by a conductance (g), kinetics with a deactivation time constant (τ_d), and short-term plasticity (ST-P) through the dynamics of synaptic resource utilization and recovery determined by three parameters: a recovery time constant (τ_r), a facilitation time constant (τ_f), and the utilization ratio (U).

Large g values lead to high synaptic amplitudes, and large τ_d values result in slow kinetics. Depending on the calcium concentration in the presynaptic terminal, each synaptic event increases resource utilization rate, reflecting the number of released neurotransmitters and of postsynaptic receptors occupied at any moment. U determines the utilization increment proportion after each event, but it is not the only factor. Resource utilization rate diminishes between events as calcium is reabsorbed. The utilization reduction pace is determined by τ_f. When τ_f is large, utilization reduction speed is slow, and synapses have a higher probability to facilitate. Since synaptic resources are limited, utilization may cause depletion. Therefore, synapses could have fewer resources for the next event, unless they recover quickly. The factor τ_r determines the recovery speed. High τ_r indicates lower recovery rate which makes synapses more likely to undergo short-term depression.

Quantifying synaptic physiology with the aforementioned parameters enable the unification of diverse experimental data. Nevertheless, different covariates including species, sex, temperature, and recording modality make it difficult to compare synapses beyond the scope of the original studies. Published reports also do not cover all potential connections. Synaptic data in Hippocampome.org are only available for ~ 84% of potential connections in the hippocampal formation. Moreover, due to the often-ambiguous identification of cell types, each synaptic signal is typically mappable to several potential connections (Fig. 1). To solve these problems, the mined data require proper integration[10]. Deep learning is a powerful tool for data integration and supports multi-target regression[11–14]. In fact, trial-to-trial heterogeneity may increase the robustness of machine learning[15]. Despite its successes in other fields, deep learning has never been employed to integrate synaptic electrophysiology data.

This study introduces a novel strategy to integrate synaptic electrophysiology data. By fitting the quantitative measurements of recorded connections with a parametric synapse model, we effectively reconciled data collected through multifarious methods. Then, we trained a predictive deep learning model to normalize the data for covariates and validated the prediction accuracy against the measured experimental variability. The model can infer missing values in arbitrary conditions and resolve ambiguous neuronal identities. Thus, for the first time, we comprehensively analyzed the normalized synaptic properties of all potential connections of the rodent entorhinal-hippocampal network and unraveled crucial factors governing synaptic physiology.

Results

We compiled, digitized, and reconstructed from the published literature a comprehensive dataset of 2,621 synaptic signals recorded from the dentate gyrus, CA3, CA2, CA1, subiculum, and entorhinal cortex. For each recording, we annotated the detailed experimental conditions with 75 covariates (Methods; Table 1) and mapped the potential pair of presynaptic and postsynaptic neuron types among 3,120 potential connections identified by Hippocampome.org (Moradi and Ascoli, 2020). While this synaptic database constitutes a uniquely information-rich resource, its quantitative analysis requires solving distinct challenges (Fig. 1). First, researchers record synaptic signals in different modalities (current- or voltage-clamp) and widely diverse experimental conditions, which cannot be directly compared. Second, synaptic measurements can rarely be ascribed to single identified presynaptic and postsynaptic neuron types: in most cases, the mapping is 'fuzzy' and matches several potential connections (green arrows in Fig. 1). Third, synaptic data are unavailable for a sizeable minority of potential connections. Additionally, certain experiments only include one synaptic event (e.g., upper right signal in Fig. 1), thus providing no information on short-term plasticity. To solve part of the first challenge (normalizing recording modality and a subset of covariates), we fit all synaptic recordings to the same model via signal simulation. To solve the remaining challenges (normalizing the rest of the covariates, disambiguating potential connections, and inferring missing data), we bring to bear an original strategy based on machine learning.

Modeling comparable synaptic parameters from diverse measures and modalities

Data integration starts with the digitization of published synaptic recordings (Fig. 2a). These signals are diverse in terms of measurement modalities (current vs voltage) and the composition of intracellular and extracellular solutions affecting reversal potentials (E_{rev}). To transform these data into a comparable form, we fitted all digitized signals to a simplified Tsodyks, Pawelzik, and Markram (TPM) model, which represents synaptic properties with 5 parameters (Supplementary Methods)[9, 16]. These synapse-specific parameters (g, τ_d, τ_r, τ_f, and U) depend on the combination of presynaptic and postsynaptic neuronal types involved and are estimated by fitting the TPM model output to the digitized signals (Fig. 2b). The model also requires a small set of measurements that depend on experimental settings and the properties of the postsynaptic neuron: E_{rev}, the initial value of the membrane voltage (V_m), membrane time constant (τ_m), and capacitance (C_m). To eliminate the impact of processes causing slow signal fluctuations, we corrected the signals before parametric fitting (Fig. S1 and Methods). The TPM model produced comparable synaptic parameters and normalized the data with respect to synaptic driving force (V_m - E_{rev}) by converting synaptic amplitudes to conductance. Overall, the process reduces data dimensionality by describing every signal with only 5 values.

Construction and validation of a predictive model of all synapses

The fitted parameters for matching potential connections in different experimental conditions reveal a large degree of variation that could be associated with covariates such as animal sex, species, recording and stimulation methods, and temperature (Fig. S2a-d). To normalize the effect of covariates, we trained a predictive deep learning model of the synaptic parameters using a five-layer autoencoder perceptron

architecture (Figs. 2c and S3; Methods). Given a potential connection and experimental covariates (i.e., features: Table 1), the models learned to infer the 5 synaptic parameters (i.e., targets). Training converged to stable performance with learned values deviating on average less than 30% from the experimental measurements (Fig. S4a). The model displayed no overfitting and the predicted values (for targets not included in the training set) deviated only marginally more (~ 32%) from the original measurements (Fig. S4a). To assess this performance relative to the reliability of experimental measurements, we consider different experimental values ("targets") recorded from the exact same nominal conditions ("features"). Those differences can be ascribed to unknown experimental factors, intrinsic biological variability, and random noise. We take such empirical ground-truth range as the "gold standard" to benchmark our model against. In these cases, we calculated the distance of each target value from their average, a measure of experimental fluctuation we call *target variability*. We compared the target variability with the training accuracy and prediction accuracy, i.e., the distance of model output from seen and unseen targets, respectively. The training and prediction accuracies of our predictive model were remarkably close to the target variability. Testing the predictive power of the model with the jackknife (leave-one-out) method, we found that the vast majority of unitary predictions fell within the 95% confidence interval of the targets, i.e., they were "reliable" (Figs. 3a-b). Specifically, this *prediction reliability* (PR) ranged from 90% for τ_r to 96% for U, with intermediate values for g (91%), τ_d (94%), and τ_f (94%). By including all synaptic measurements (not just the unitary values, PR was reduced slightly to 88%-94% (Figs. S4b-d). Additionally, comparing the relevant values to sparse estimates available for matching potential connections from a recent CA1 study[17] revealed no statistically significant difference for any of the 5 parameters (Fig. S5). Thus, the deep learning model quantitatively predicts the properties of synaptic signals for which experimental recordings are available within the margin of measurement accuracy.

Connectivity matrix completion and synaptic data normalization

Given its demonstrated performance on available data, the predictive model can confidently estimate the synaptic parameters of yet uncharacterized potential connections based on the learned properties of neuronal types. The model can complete the synaptic electrophysiology matrix for all 3,120 potential connections in the hippocampus and entorhinal cortex. Additionally, since the learned neuronal properties are all unique, the model also effectively disambiguates each potential connection: in other words, the predicted synaptic parameters for each pair of neuron types are also all unique. Importantly, the deep learning model can infer synaptic parameters for every potential connection in any desired condition. Applying homogeneous conditions for all potential connections practically normalizes the inferences with respect to the covariates. This study primarily focuses on fast unitary synaptic properties in near-physiological (henceforth "standard") condition, namely AMPA and GABA$_A$ synapses of adult male rats in voltage-clamp at body temperature and with a pipette solution that does not disturb intracellular ionic concentrations (Methods). These so-derived synaptic signals showed a wide range of amplitudes, kinetics, and ST-P across potential connections (Fig. 3c and Suppl. Video). To explore regional differences within the hippocampal formation, we inspected the probability density distributions of all parameter values normalized using the min-max method (Fig. S6a). Interestingly, the range of values in the

entorhinal cortex is smaller than in the hippocampus. Moreover, the GABAergic and the glutamatergic synapses had overlapping distributions for g and U but not for the time constants (Fig. S6b), suggesting that these synapse types have similar amplitudes but differ in kinetics and ST-P.

Open access to data and source codes

The normalized and completed synaptic data are broadly applicable to designing experiments in optimal conditions, testing hypotheses, constraining biologically plausible simulations of the entire entorhinal-hippocampal circuit[18], and benchmarking machine learning algorithms. We provide 5 synaptic constants for each of 3,120 connections in 32 different settings that include all binary combinations of species (rat or mouse), sex (male or female), age (young or adult), recording method (voltage- or current-clamp), and temperature (room or body). For each parameter we make available the mean, standard deviation, and range over 100 training runs of the deep learning model (Fig. 4a). We also share all implemented tools for unhindered reuse with other datasets. The Synapse Modeling Utility, the preprocessing and analysis code in R, the machine learning library in Python, and the preprocessed machine learning-ready experimental data (2,621 features-targets sets) are all freely available on Hippocampome.org/synapse (Fig. 4b).

Presynaptic and postsynaptic determinants of synaptic physiology

Full data normalization allowed us to compare for the first time the synaptic properties of all potential connections without the influence of confounding variables. To begin the investigation of how the presynaptic and postsynaptic identities combine to define synaptic dynamics, we asked two questions: (1) when a pair of neuron types forms a synapse, which synaptic properties (e.g., amplitude, duration, ST-P) does either side dominantly determine? (2) Does the answer differ for glutamatergic and GABAergic synapses? To answer these questions, we separated the glutamatergic and GABAergic synapses. In each pool, we created two groupings: one based on the presynaptic neuron types, and the other based on the postsynaptic ones. For example, the glutamatergic presynaptic grouping consisted of 38 groups, one for every glutamatergic presynaptic type; each of these groups contains all postsynaptic neuron types that presynaptic type forms a connection with. We then calculated for each group the coefficient of variation (CV) of all 5 synaptic parameters in the standard condition (Fig. 5a). A lower CV indicates less intragroup variation and thus a tighter control of the corresponding grouping on that synaptic property. For GABAergic synapses, the ST-P parameters (but not conductance and kinetics) had significantly smaller CVs if synapses were grouped based on postsynaptic type. For glutamatergic synapses, in contrast, all parameters except U had significantly smaller CVs if synapses were grouped based on presynaptic type. In other words, presynaptic glutamatergic neurons and postsynaptic $GABA_A$ receptors are more important determinants of synaptic signals.

Principal covariate effects on synaptic properties

Next, we systematically investigated the influence of experimental covariates on synaptic parameters. Earlier research mainly checked the impact of experimental conditions on synaptic amplitude and kinetics of a limited number of neuron types. Our study also allowed the inclusion of ST-P parameters

and systematically covered all potential connections of the hippocampal formation by changing one covariate at a time. All tested covariates had a statistically significant impact on synaptic parameters, but we only report here (Fig. 5b-c) those with a meaningful effect size (> 10%) and emphasize the most substantive ones (> 20%). Our results indicate that g increases more than two-fold and τ_d decreases 30% when switching from voltage- to current-clamp, from male to female animals, and from gluconate-free to gluconate-containing intracellular solutions. While the change with recording modality agrees with previous studies for example, [19] and we expected a difference by sex, the pronounced impact of gluconate in the pipette solution was surprising. Moreover, current clamp (relative to voltage clamp) and female animals (relative to male) also entailed notably higher τ_r and lower τ_f, implying greater propensity towards synaptic depression. In contrast, the opposite trend, conducive to facilitation, was observed with gluconate. Shifting from rats to mice or from room to body temperature affected synaptic properties in the same direction, but to a more modest extent (10–20% effect size), as the male-to-female switch or intracellular gluconate addition, respectively. Reducing $[Cl]_i$ substantially increased short-term facilitation at GABAergic synapses, while more modestly slowing down synaptic kinetics which was unexpected based on [20]. Other covariates, including to our surprise age, did not affect the parameters substantially. Altogether, remarkably, only two types of variation, differing just in the change direction of τ_r and τ_f, could explain the impact of all analyzed covariates irrespective of neurotransmitter type. This observation suggests an interdependence among synaptic parameters.

Synaptic amplitude predicts signal kinetics and the direction of short-term plasticity

Among both glutamatergic and GABAergic types, we noticed that synapses with high amplitude had fast kinetics and demonstrated depressing ST-P. Conversely, synapses with low amplitude had slower kinetics and were facilitating. To visualize these observations, we averaged the model parameters from the 30 synapses with the largest conductance and from the 30 with the smallest one among both glutamatergic and GABAergic groups. We then compared the responses of the four consensus models in standard condition (Fig. 6a and Suppl. Video). The high-amplitude models exhibited short-term depression and short signal duration (half-height width: 2.4 ms for glutamatergic and 3.8 ms for GABAergic), while the low-amplitude models demonstrated short-term facilitation and long signal duration (half-height width: 5.1 ms for glutamatergic and 6.2 ms for GABAergic). Considering all 3,120 connections revealed a significant negative correlation between g and τ_d and between g and the paired-pulse ratio from baseline of the third synaptic event ($AB_3:A_1$), but a positive correlation between g and U, suggesting that high-amplitude synapses have higher resource utilization (Fig. 6b). Facilitation and depression partly depend on interstimulus intervals (ISI) and the measure of ST-P. Testing ST-P at 20 ms ISI and considering $AB_3:A_1$, the majority (> 90%) of synapses with amplitude below 0.5 nS facilitated, irrespective of neurotransmitter, while most synapses above 2 nS (glutamatergic) or 3 nS (GABAergic) depressed (Fig. 6c, left). Although the second synaptic events (AB2:A1) tended towards facilitation relative to subsequent signals (e.g., AB5:A1), all ST-P measures consistently transitioned from facilitation to depression as a function of conductance (Fig. 6c, right). Moreover, τ_f and τ_r were negatively correlated (R_{glu}=-0.4, R_{GABA}=-0.1, $p < 0.05$), indicating that synapses needing a long time to recover their resources tend to reduce their synaptic

utilization rate rapidly. Altogether, these analyses suggest that higher synaptic amplitudes predict faster kinetics and a tendency towards depression over facilitation, reflecting coordinated differences in τ_d and U as well as interdependence of τ_f and τ_r.

Presynaptic and postsynaptic molecular expression as a biomarker of short-term plasticity

It is a widespread practice to study synapses based on molecular expression. Chemical biomarkers were not directly among the training features of our predictive synapse models, but were used for mapping mined signals to potential connections[8]. We employed Hippocampome.org to query neuron types expressing different markers[21, 22] and analyzed differences in synaptic properties among neuron types containing (+) or lacking (-) each molecule. Since certain markers are expressed in the presynaptic terminals and others in the postsynaptic dendrites and soma[23], we studied the presynaptic and the postsynaptic groups separately (Fig. 7). Considering $AB_3{:}A_1$ as a measure of ST-P and using a 20 ms ISI, we identified two classes of presynaptic markers that respectively predicted synaptic facilitation and depression. Specifically, presynaptic calbindin (CB), cholecystokinin (CCK), and neuropeptide-Y (NPY) expression correlated with facilitation (larger $AB_3{:}A_1$ values). In contrast, calretinin (CR), parvalbumin (PV), and somatostatin (SOM) correlated with depression (smaller $AB_3{:}A_1$ values). The relations of these markers with changes in synaptic amplitude and kinetics were not always statistically significant but generally followed the trends revealed in the previous section: namely, presynaptic expressions predicting short-term facilitation typically demonstrated lower signal amplitudes and slower kinetics and vice versa for those predicting short-term depression. Cannabinoid receptor 1 (CB1) is expressed both on presynaptic and postsynaptic sides[24]. Since the presynaptic effects were similar to CCK, we only illustrated the postsynaptic effects. Among the postsynaptic markers, both CB1 and serotonin receptor 3 (5HT-3) predicted lower amplitudes and a tendency towards facilitation. Interestingly, CB1 exerted greater impact when partnering with GABAergic than with glutamatergic synapses.

Correlations between neuronal morphology and synaptic parameters

In GABAergic neurons of both hippocampal area CA1 and visual cortex, the kinetics of spontaneous synaptic inputs vary depending on the specific axonal targeting of that same postsynaptic neuron[25, 26]. We tested similar interactions between input synaptic properties and output axonal patterns throughout the hippocampal formation, not only considering unitary synaptic kinetics, but also conductance and ST-P (Fig. S7). Among GABAergic synapses in CA1, we found significant differences in g, τ_d, τ_f, and U, indicating that not only input synaptic duration, but also amplitude and facilitation, vary by output axonal targeting (Fig. S7a). Extending the study to other hippocampal regions revealed significant differences in τ_d and τ_f among GABAergic synapses in CA3, and in τ_r in DG and CA2. Glutamatergic synapses generally demonstrated fewer significant differences. Visualizing consensus traces (Fig. S7b) and synaptometrics differences (Fig. S7c) confirmed these patterns.

In the visual cortex, connection probability correlates with synaptic strength[27]. Hippocampome.org calculates the probabilities of connections and the average synaptic distance from the presynaptic and postsynaptic soma based on the layer-specific linear densities of the corresponding axons and dendrites [28]. Synaptic conductance had a weak but significant positive correlation with the connection probability (R_{GABA}=0.27, R_{Glu}=0.19, $p < 0.05$). Consistent with dendritic filtering, we also found a significantly negative correlation between g and the synaptic distance from the postsynaptic soma (R_{GABA}=-0.13, R_{Glu}=-0.06, $p < 0.05$).

Discussion

We digitized, reconstructed, and compiled a comprehensive dataset of 2,621 synaptic signals recorded from the rodent hippocampus and entorhinal cortex, and mapped each to respective covariates and potential connections. Through computational modeling and machine learning, we normalized and completed for the first time all synaptic physiology data to predict the amplitude, kinetics, and ST-P of the 3,120 potential connections of the hippocampal formation. For each potential connection, we freely released via Hippocampome.org the complete set of 5 synaptic parameters in 32 different experimental settings with all annotated experimental data, plus analysis and modeling software source code. We identified the major determinants of unitary synaptic physiology and discovered new correlations among synaptic properties, molecular expression, and neuronal morphology.

Application of machine learning to data normalization and completion

Broad diversity in experimental settings causes extreme variability in synaptic electrophysiological recording. Combined with inherent measurement noise, this makes identifying causal relations among variables considerably challenging. To our knowledge, our application of deep learning to solve these issues is the first of its kind in neuroscience. Testing the deep learning model with unseen data demonstrated that the predictions are valid within experimental accuracy. Applying uniform experimental conditions (voltage-clamp at body temperature in male rats with specified intra- and extra-cellular solutions) to all potential connections effectively normalized data. In that scenario, the only differences in synaptic parameters are due to the presynaptic and postsynaptic neuron identities. At the same time, changing the chosen experimental condition, such as switching from male to female animals, allows the systematic investigation of every covariate effect.

Furthermore, our novel deep learning solution yields two notable *data augmentation* benefits. First, it fills in missing data by matrix completion harnessing the learned axonal and dendritic properties of the corresponding neuron types. In simple terms, if the predictive model learns synaptic features from neuron type x to neuron type y, and from type w to type z, it can then infer the features from x to z and from w to y based on the axonal properties of x and w and the dendritic properties of y and z. In reality, the known features utilized in training are more numerous than the set of missing data. For comparison, an earlier study measured the synaptic physiology of 10% of potential connections in CA1 to extrapolate the properties of the remaining 90% based on marker profiles [17]. In contrast, our experimental dataset

covered the majority of potential connections across the entire hippocampal formation, with missing values ranging from 16.3% for conductance to 38.5% for ST-P. Singular value decomposition (SVD) may robustly complete matrices with up to 50% of missing values[29], but deep learning typically outperforms SVD in this process[11].

The second beneficial effect of our machine learning approach is that it leverages data redundancy to disambiguate the mappings of individual signals to multiple potential connections. Consider for instance an experimental recording mapped to potential connections A or B and a different recording mapped to potential connections B or C; the deep learning model utilizes the two constraints on B to predict a unique set of synaptic parameter values distinct from those of A and C. Indeed, the inferred values were all different for the 3120 pairs of hippocampal neuron types, indicating that the training data was sufficient to completely resolve degenerate mappings.

Larger synaptic conductance entails faster decay and resource exhaustion

The synapses of the entorhinal-hippocampal network communicate through a broad continuum of signal amplitudes. Yet, the sets of neurotransmitters and receptors employed by this circuit are limited, raising a question: *does variation in synaptic conductance interact with resource utilization and recovery to affect kinetics and ST-P?* Unnormalized unitary data suggest that kinetics are faster for strong GABAergic synapses than for weak ones[8]. Additionally, one study on three synapse types suggests that the ST-P of stronger synapses is depressing, and the ST-P of weaker synapses is facilitating [30]. Indeed, analyzing all potential connections of the hippocampal formation revealed a negative correlation of g with both τ_d and $AB_3:A_1$. Moreover, we found a positive correlation between g and U, consistent with the TPM model (Eq. 13 in Suppl. Methods). Since U quantifies the utilization increment, these results suggest that high-amplitude synapses depress more easily because of resource exhaustion.

Synaptic dynamics reveal economic resource usage and limited degree of freedom

The TPM model accounts for resource utilization and recovery. When τ_r is small, resource recovery pace is fast. When τ_f is large, resource utilization remains prolonged. Therefore, the opposite dependence of τ_f and τ_r on covariates indicates that *when resource recovery pace is fast, resource spending is prolonged*. Furthermore, their higher negative correlation in glutamatergic synapses relative to GABAergic ones suggests that resource utilization is subject to tighter control in the former than in the latter. Overall, the effects of covariates on synaptic parameters revealed only two distinct patterns that differed exclusively in the change direction of τ_r and τ_f. The mere simplicity of these observations could be explained by the correlation among synaptic parameters. Covariates increasing g will also increase U and decrease τ_d. The only remaining freedom is in τ_r and τ_f, which always change in opposite directions. This suggests that *covariates affect a small set of latent variables*.

Synaptic parameters depend on sex and recording method more than on species

For equivalent experimental conditions and irrespective of neurotransmitter, female animals had, relative to males, multiplicatively larger unitary synaptic conductance, significantly faster kinetics, and greater tendency towards short-term depression than facilitation. It is tempting to speculate a link to chronic exposure to neurosteroids and endocannabinoids, which increase the amplitudes of glutamatergic and GABAergic synapses, respectively, in females[31–33]. We observed similar changes in synaptic parameters when switching from voltage-clamp to current-clamp. This could be due to the activation of voltage-gated ion channels in current-clamp or the reduction of passive filtering during parametric fitting that brings the estimations closer to the local dendritic event[19,34]. We also found qualitatively parallel differences between species, with significantly larger synaptic conductance in mice compared to rats. Notwithstanding the high statistical sensitivity of our study, however, the phenomenological disparity across rodents was practically negligible (see Suppl. Material for further considerations).

Intracellular gluconate is a potent synaptic enhancer

The common food additive potassium gluconate (E577), when added to the patch-clamp intracellular solution, changes the reversal potential of $GABA_A$ channels[35], blocks ion channels involved in subthreshold membrane physiology[36], and alters firing patterns in hippocampal neurons[37]. However, the impact of intracellular gluconate on unitary synaptic signaling has never been studied systematically. We found intracellular gluconate to be one of the most potent synaptic enhancers. With gluconate in the recording pipette, synaptic amplitudes were a fold-factor larger, kinetics were faster, and short-term plasticity shifted from depression to facilitation (smaller τ_r and larger τ_f). The increment of synaptic amplitude could be explained by blockage of the subthreshold channels, which reduces shunting and increases input resistance. The reduction of short-term depression may be due to the role of gluconate as an energy source that facilitates resource recovery. As a comparison, the effect of gluconate on synaptic parameters was a full order of magnitude larger than the changes observed in the same direction when shifting from room temperature to body temperature.

Presynaptic and postsynaptic predictors of synaptic properties

Our data analysis suggests that the presynaptic side of glutamatergic, and the postsynaptic side of GABAergic neurons, have a relatively higher impact on synaptic properties. For GABAergic synapses, this finding could be explained by the selective targeting of Axo-axonic and Interneuron Specific neurons[6]. At the same time, each neuron type in Hippocampome.org is linked to known molecular biomarkers expressed either in the axons (e.g. calcium-binding proteins and neuropeptides) or in the dendrites (e.g. neurotransmitter receptors). Among calcium-binding proteins, calbindin was a biomarker of facilitating synapses while calretinin and parvalbmin of depressing ones. Among neuropeptides, CCK and NPY marked a tendency toward facilitation and somatostatin towards depression. Among neurotransmitter receptors, cannabinoid receptor 1 and serotonin-gated ionotropic channels altered synaptic properties similarly. While this result is consistent with their pattern of co-expression in cortical neurons[38], their underlying mechanisms are likely distinct given the specific dendritic compartmentalization of 5-HT3, but not of CB1.

Conclusion

Experimental synaptic recordings can be properly integrated by computational modeling and deep learning to provide the normalized, completed, and disambiguated unitary electrophysiology data of all potential connections in the hippocampal formation in any desired setting. These data can be used to test hypotheses, constrain and validate realistic computer simulations, and optimize experimental design. The devised method and tools are also applicable to the quantitative investigation of synaptic data in other brain regions and species.

Methods

Due to technical limitations, the methods section is only available as a download in the supplementary files section.

Declarations

Acknowledgments

Competing interests: The authors declare no competing interests

References

1. DeFelipe, J. From the connectome to the synaptome: an epic love story. *Science* **330**, 1198-1201 (2010).
2. Nanou, E. & Catterall, W.A. Calcium Channels, Synaptic Plasticity, and Neuropsychiatric Disease. *Neuron* **98**, 466-481 (2018).
3. Grant, S.G.N. Synapse diversity and synaptome architecture in human genetic disorders. *Hum Mol Genet* **28**, R219-R225 (2019).
4. Moradi, K. & Ascoli, G.A. Systematic data mining of hippocampal synaptic properties. in *Hippocampal Microcircuits A Computational Modeler's Resource Book* (ed. V. Cutsuridis, B.P. Graham, S. Cobb & I. Vida) 441-471 (Springer International Publishing, Switzerland, 2019).

5. Ascoli, G.A. & Wheeler, D.W. In search of a periodic table of the neurons: Axonal-dendritic circuitry as the organizing principle: Patterns of axons and dendrites within distinct anatomical parcels provide the blueprint for circuit-based neuronal classification. *Bioessays* **38**, 969-976 (2016).

6. Rees, C.L., Moradi, K. & Ascoli, G.A. Weighing the Evidence in Peters' Rule: Does Neuronal Morphology Predict Connectivity? *Trends in neurosciences* **40**, 63-71 (2017).

7. Wheeler, D.W., *et al.* Hippocampome.org: a knowledge base of neuron types in the rodent hippocampus. *eLife* **4** (2015).

8. Moradi, K. & Ascoli, G.A. A comprehensive knowledge base of synaptic electrophysiology in the rodent hippocampal formation. *Hippocampus* **30**, 314-331 (2020).

9. Morrison, A., Diesmann, M. & Gerstner, W. Phenomenological models of synaptic plasticity based on spike timing. *Biological cybernetics* **98**, 459-478 (2008).

10. Lazebnik, Y. Can a biologist fix a radio?--Or, what I learned while studying apoptosis. *Cancer Cell* **2**, 179-182 (2002).

11. Fan, J. & Chow, T. Deep learning based matrix completion. *Neurocomputing* **266**, 540-549 (2017).

12. Stulp, F. & Sigaud, O. Many regression algorithms, one unified model: A review. *Neural networks : the official journal of the International Neural Network Society* **69**, 60-79 (2015).

13. Richards, B.A., *et al.* A deep learning framework for neuroscience. *Nature neuroscience* **22**, 1761-1770 (2019).

14. Faust, O., Hagiwara, Y., Hong, T.J., Lih, O.S. & Acharya, U.R. Deep learning for healthcare applications based on physiological signals: A review. *Comput Methods Programs Biomed* **161**, 1-13 (2018).

15. Van Hulse, J. & Khoshgoftaar, T. Knowledge discovery from imbalanced and noisy data. *Data & Knowledge Engineering* **68**, 1513-1542 (2009).

16. Tsodyks, M., Pawelzik, K. & Markram, H. Neural networks with dynamic synapses. *Neural Comput* **10**, 821-835 (1998).

17. Ecker, A., *et al.* Data-driven integration of hippocampal CA1 synaptic physiology in silico. *Hippocampus* **30**, 1129-1145 (2020).

18. Venkadesh, S., Komendantov, A.O., Wheeler, D.W., Hamilton, D.J. & Ascoli, G.A. Simple models of quantitative firing phenotypes in hippocampal neurons: Comprehensive coverage of intrinsic diversity. *PLoS Comput Biol* **15**, e1007462 (2019).

19. Beaulieu-Laroche, L. & Harnett, M.T. Dendritic Spines Prevent Synaptic Voltage Clamp. *Neuron* **97**, 75-82 e73 (2018).

20. Succol, F., Fiumelli, H., Benfenati, F., Cancedda, L. & Barberis, A. Intracellular chloride concentration influences the GABAA receptor subunit composition. *Nat Commun* **3**, 738 (2012).

21. Hamilton, D.J., White, C.M., Rees, C.L., Wheeler, D.W. & Ascoli, G.A. Molecular fingerprinting of principal neurons in the rodent hippocampus: A neuroinformatics approach. *J Pharm Biomed Anal* **144**, 269-278 (2017).

22. White, C.M., Rees, C.L., Wheeler, D.W., Hamilton, D.J. & Ascoli, G.A. Molecular expression profiles of morphologically defined hippocampal neuron types: Empirical evidence and relational inferences. *Hippocampus* **30**, 472-487 (2020).

23. Rees, C.L., White, C.M. & Ascoli, G.A. Neurochemical Markers in the Mammalian Brain: Structure, Roles in Synaptic Communication, and Pharmacological Relevance. *Curr Med Chem* **24**, 3077-3103 (2017).

24. Busquets-Garcia, A., Bains, J. & Marsicano, G. CB1 Receptor Signaling in the Brain: Extracting Specificity from Ubiquity. *Neuropsychopharmacology* **43**, 4-20 (2018).

25. Cossart, R.*, et al.* Interneurons targeting similar layers receive synaptic inputs with similar kinetics. *Hippocampus* **16**, 408-420 (2006).

26. Dumitriu, D., Cossart, R., Huang, J. & Yuste, R. Correlation between axonal morphologies and synaptic input kinetics of interneurons from mouse visual cortex. *Cerebral cortex* **17**, 81-91 (2007).

27. Jiang, X.*, et al.* Principles of connectivity among morphologically defined cell types in adult neocortex. *Science* **350**, aac9462 (2015).

28. Tecuatl, C., Wheeler, D.W., Sutton, N. & Ascoli, G.A. Comprehensive estimates of potential synaptic connections in local circuits of the rodent hippocampal formation by axonal-dendritic overlap. *The Journal of neuroscience : the official journal of the Society for Neuroscience* (2020).

29. Zeng, W. & So, H.C. Outlier-Robust Matrix Completion via lp-Minimization. *IEEE Transactions on Signal Processing* **66**, 1125-1140 (2018).

30. Toth, K., Suares, G., Lawrence, J.J., Philips-Tansey, E. & McBain, C.J. Differential mechanisms of transmission at three types of mossy fiber synapse. *The Journal of neuroscience : the official journal of the Society for Neuroscience* **20**, 8279-8289 (2000).

31. Oberlander, J.G. & Woolley, C.S. 17beta-Estradiol Acutely Potentiates Glutamatergic Synaptic Transmission in the Hippocampus through Distinct Mechanisms in Males and Females. *The Journal of neuroscience : the official journal of the Society for Neuroscience* **36**, 2677-2690 (2016).

32. Fester, L. & Rune, G.M. Sexual neurosteroids and synaptic plasticity in the hippocampus. *Brain research* **1621**, 162-169 (2015).

33. Higuera-Matas, A.*, et al.* Sex-specific disturbances of the glutamate/GABA balance in the hippocampus of adult rats subjected to adolescent cannabinoid exposure. *Neuropharmacology* **62**, 1975-1984 (2012).

34. Moradi, K., Kaka, G. & Gharibzadeh, S. The role of passive normalization, voltage-gated channels and synaptic scaling in site-independence of somatic EPSP amplitude in CA1 pyramidal neurons. *Neuroscience Research* **73**, 8-16 (2012).

35. Fatima-Shad, K. & Barry, P.H. Anion permeation in GABA- and glycine-gated channels of mammalian cultured hippocampal neurons. *Proc Biol Sci* **253**, 69-75 (1993).

36. Velumian, A.A., Zhang, L., Pennefather, P. & Carlen, P.L. Reversible inhibition of IK, IAHP, Ih and ICa currents by internally applied gluconate in rat hippocampal pyramidal neurones. *Pflugers Arch* **433**, 343-350 (1997).

37. Komendantov, A.O._, et al._ Quantitative firing pattern phenotyping of hippocampal neuron types. _Sci Rep_ **9**, 17915 (2019).

38. Morales, M., Wang, S.D., Diaz-Ruiz, O. & Jho, D.H. Cannabinoid CB1 receptor and serotonin 3 receptor subunit A (5-HT3A) are co-expressed in GABA neurons in the rat telencephalon. _The Journal of comparative neurology_ **468**, 205-216 (2004).

39. Yu, J., Swietek, B., Proddutur, A. & Santhakumar, V. Dentate total molecular layer interneurons mediate cannabinoid-sensitive inhibition. _Hippocampus_ **25**, 884-889 (2015).

40. Szabadics, J. & Soltesz, I. Functional specificity of mossy fiber innervation of GABAergic cells in the hippocampus. _The Journal of neuroscience : the official journal of the Society for Neuroscience_ **29**, 4239-4251 (2009).

41. Gloveli, T._, et al._ Differential involvement of oriens/pyramidale interneurones in hippocampal network oscillations in vitro. _The Journal of physiology_ **562**, 131-147 (2005).

42. Glickfeld, L.L. & Scanziani, M. Distinct timing in the activity of cannabinoid-sensitive and cannabinoid-insensitive basket cells. _Nature neuroscience_ **9**, 807-815 (2006).

43. Elfant, D., Pal, B.Z., Emptage, N. & Capogna, M. Specific inhibitory synapses shift the balance from feedforward to feedback inhibition of hippocampal CA1 pyramidal cells. _The European journal of neuroscience_ **27**, 104-113 (2008).

44. Couey, J.J._, et al._ Recurrent inhibitory circuitry as a mechanism for grid formation. _Nature neuroscience_ **16**, 318-324 (2013).

45. Le Duigou, C., Savary, E., Kullmann, D.M. & Miles, R. Induction of Anti-Hebbian LTP in CA1 Stratum Oriens Interneurons: Interactions between Group I Metabotropic Glutamate Receptors and M1 Muscarinic Receptors. _The Journal of neuroscience : the official journal of the Society for Neuroscience_ **35**, 13542-13554 (2015).

46. Mercer, A., Eastlake, K., Trigg, H.L. & Thomson, A.M. Local circuitry involving parvalbumin-positive basket cells in the CA2 region of the hippocampus. _Hippocampus_ **22**, 43-56 (2012).

47. Akima, H. A new method of interpolation and smooth curve fitting based on local procedures. _Journal of the ACM (JACM)_ **17**, 589-602 (1970).

48. Savanthrapadian, S._, et al._ Synaptic properties of SOM- and CCK-expressing cells in dentate gyrus interneuron networks. _The Journal of neuroscience : the official journal of the Society for Neuroscience_ **34**, 8197-8209 (2014).

49. Kraushaar, U. & Jonas, P. Efficacy and stability of quantal GABA release at a hippocampal interneuron-principal neuron synapse. _The Journal of neuroscience : the official journal of the Society for Neuroscience_ **20**, 5594-5607 (2000).

50. Bartos, M., Vida, I., Frotscher, M., Geiger, J.R. & Jonas, P. Rapid signaling at inhibitory synapses in a dentate gyrus interneuron network. _The Journal of neuroscience : the official journal of the Society for Neuroscience_ **21**, 2687-2698 (2001).

51. Hines, M.L. & Carnevale, N.T. The NEURON simulation environment. _Neural Comput_ **9**, 1179-1209 (1997).

52. Misra, D. Mish: A self regularized non-monotonic neural activation function. *arXiv preprint arXiv:1908.08681* (2019).

53. Hinton, G.E., Srivastava, N., Krizhevsky, A., Sutskever, I. & Salakhutdinov, R.R. Improving neural networks by preventing co-adaptation of feature detectors. *arXiv preprint arXiv:1207.0580* (2012).

54. Srivastava, N., Hinton, G., Krizhevsky, A., Sutskever, I. & Salakhutdinov, R. Dropout: a simple way to prevent neural networks from overfitting. *The journal of machine learning research* **15**, 1929-1958 (2014).

55. Ioffe, S. & Szegedy, C. Batch normalization: Accelerating deep network training by reducing internal covariate shift. *arXiv preprint arXiv:1502.03167* (2015).

56. Loshchilov, I. & Hutter, F. Decoupled weight decay regularization. *arXiv preprint arXiv:1711.05101* (2017).

57. Li, Y. & Liu, F. Whiteout: Gaussian Adaptive Noise Regularization in Deep Neural Networks. *arXiv preprint arXiv:1612.01490* (2016).

58. Prechelt, L. Early stopping-but when? in *Neural Networks: Tricks of the trade* 55-69 (Springer, 1998).

59. Hyndman, R.J. & Koehler, A.B. Another look at measures of forecast accuracy. *International journal of forecasting* **22**, 679-688 (2006).

60. Ribeiro, M., da Silva, R.G., Mariani, V.C. & Coelho, L.D.S. Short-term forecasting COVID-19 cumulative confirmed cases: Perspectives for Brazil. *Chaos Solitons Fractals* **135**, 109853 (2020).

61. Zhang, M., Lucas, J., Ba, J. & Hinton, G.E. Lookahead optimizer: k steps forward, 1 step back. in *Advances in Neural Information Processing Systems* 9597-9608 (2019).

62. Rodriguez, J.D., Perez, A. & Lozano, J.A. Sensitivity analysis of k-fold cross validation in prediction error estimation. *IEEE transactions on pattern analysis and machine intelligence* **32**, 569-575 (2009).

63. Bengio, Y. & Grandvalet, Y. No unbiased estimator of the variance of k-fold cross-validation. *Journal of machine learning research* **5**, 1089-1105 (2004).

64. Benjamini, Y. & Hochberg, Y. Controlling the false discovery rate: a practical and powerful approach to multiple testing. *Journal of the Royal statistical society: series B (Methodological)* **57**, 289-300 (1995).

65. Lusa, L., Miceli, R. & Mariani, L. Estimation of predictive accuracy in survival analysis using R and S-PLUS. *Comput Methods Programs Biomed* **87**, 132-137 (2007).

66. Canty, A. & Ripley, B. boot: Bootstrap R (S-Plus) functions. *R package version* **1**, 3-20 (2017).

Figures
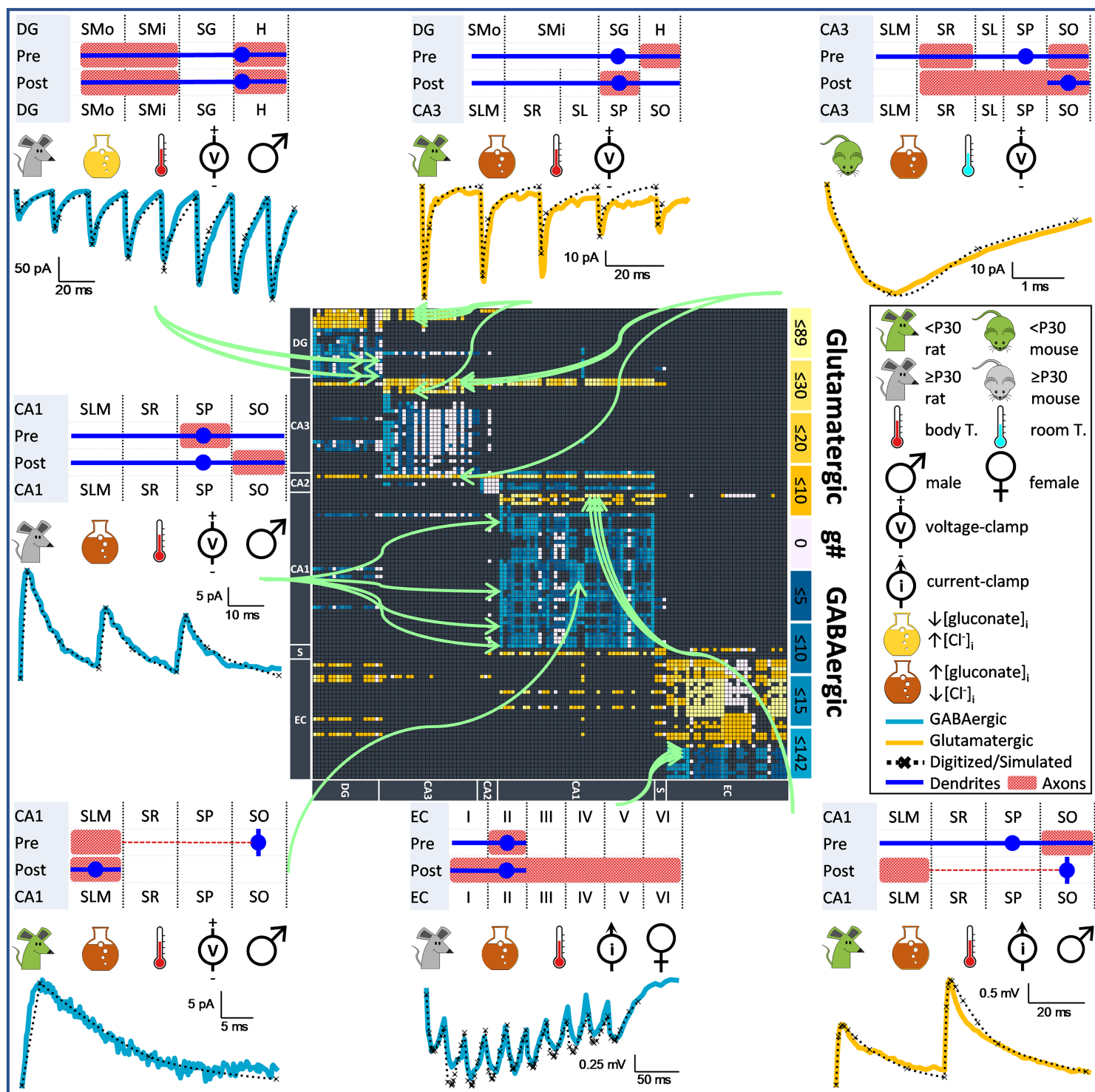
Figure 1

Diversity of synaptic covariates and mapping degeneracy. Examples of synaptic signals mined from peer-reviewed studies (solid lines: blue, GABAergic; gold, glutamatergic) and corresponding digitized reconstruction (dotted lines). Each signal is mapped to the possible presynaptic and postsynaptic neuron types (schematic morphologies) based on their axonal (red pattern) and soma-dendritic (blue dot and line) distributions across layers (SMo/SMi, outer/inner molecular; SG, granule; H, hilus; SLM, lacunosum-moleculare; SR, radiatum; SL, lucidum; SP, pyramidal; SO, oriens). We only illustrated the most likely

neuron types. The green arrows point to all possible mappings for every signal into the matrix of 3,120 potential connections (rows: presynaptic, columns: postsynaptic) among 122 neuron types. Blue and gold brightness in the connectivity matrix indicate the number of available experimental recordings. Light pink entries are potential connections with missing synaptic data. Black entries mark the absence of potential connection. The icons illustrate a sample of experimental covariates: species, age, sex, recording temperature and modality, and relative intracellular anionic concentrations. Top left, recording between a pair of dentate gyrus (DG) MOLAX or DG Total Moleculare Layer interneurons39. Top middle, signal from a DG Granule cell (or CA3 Granule, DG Semilunar Granule, or DG Hilar Ectopic Granule cell) to a CA3 Basket CCK+ cell40. Top right, signal from a CA3 Pyramidal (or CA3c Pyramidal cell) to a CA3 Trilaminar (or CA3 Interneuron Specific Oriens) cell41. Middle left, signal from a CA1 Basket CCK+ (or CA1 Radial Trilaminar, CA1 Oriens/Alveus, or CA1 Schaffer Collateral-Associated) cell to a CA1 Pyramidal cell42. Lower left, signal from a CA1 O-LM cell to a CA1 Neurogliaform cell43. Lower middle, signal from an entorhinal cortex (EC) LII Basket-Multipolar (or EC LII Axo-Axonic or medial EC LII Basket) cell to a medial EC LII Stellate neuron44. Lower right, signal from a CA1 Pyramidal cell to a CA1 O-LM (or CA1 Recurrent O-LM, or CA1 O-LMR) cell45.
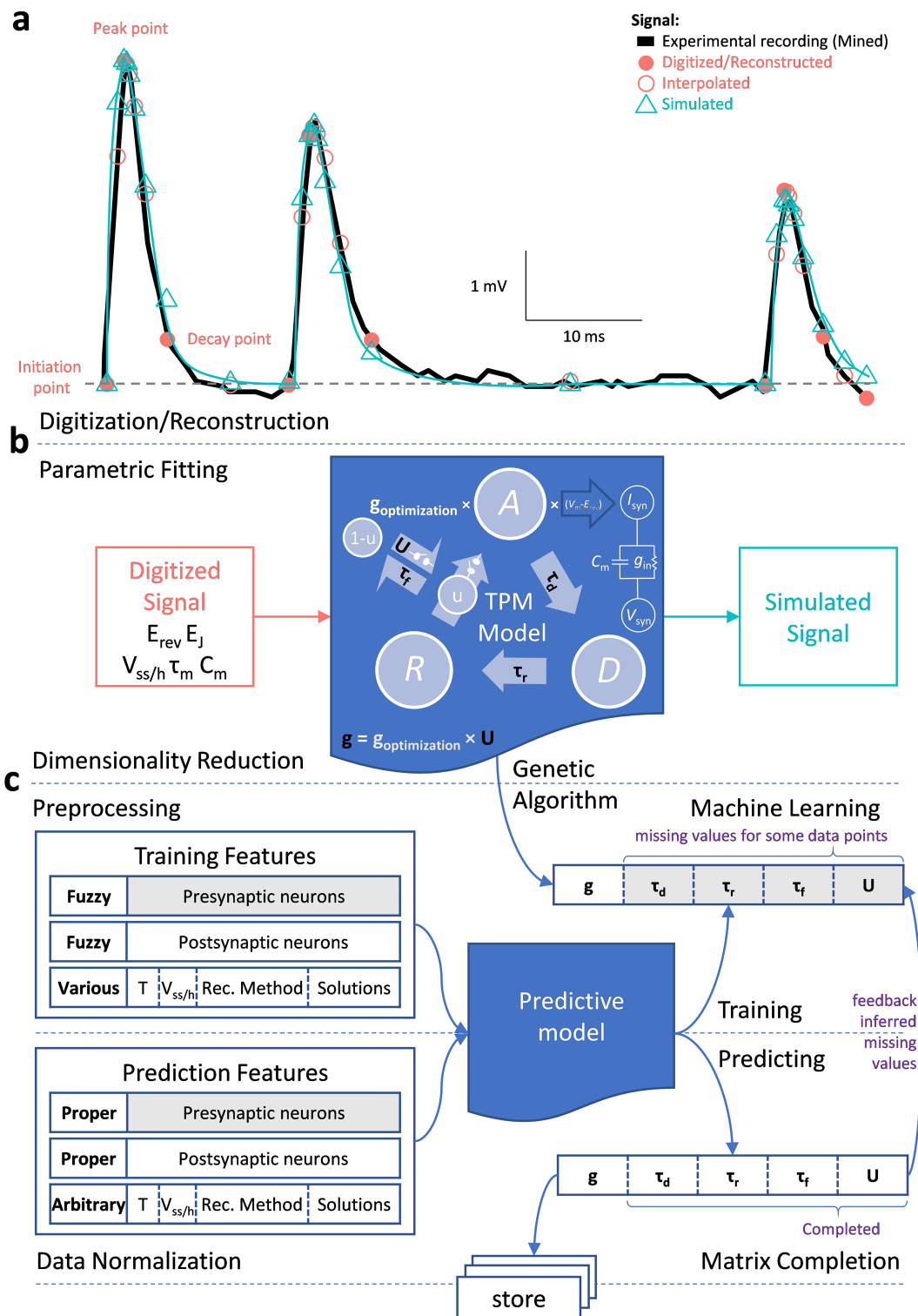
Figure 2

Synaptic modeling and deep learning. (a) Digitized trace (black line) from a CA2 Pyramidal cell to a CA2 Narrow-Arbor Basket PV+ cell46. The corresponding 9-point reconstruction of each spike (red circles), based on initiation, peak, decay (filled circles), and 6 interpolations (hollow circles), are used to optimize the simulated signal (green). (b) The Tsodyks-Pawelzik-Markram (TPM) model describes synaptic amplitude, kinetics, and short-term plasticity in terms of utilization rate (u), activation (A), deactivation

(D), and recovery (R) dynamics using experimentally measured reversal potential (Erev), junction potential (Ej), holding potential (Vh), steady-state potential (Vss), membrane time constant (τm), and membrane capacitance (Cm). A genetic algorithm yields the best-fitting values of 5 synapse-specific parameters: conductance (g), single-exponential decay time constant (τd), recovery time constant (τr), facilitation time constant (τf), and utilization ratio (U). (c) The predictive machine learning model of synaptic electrophysiology used a deep learning architecture with five hidden layers and error backpropagation. The input layer encoded the (typically fuzzy) presynaptic and postsynaptic neuron types (122×2 nodes) and all covariates (75 nodes). The output layer consisted of one node for each of the 5 synapse-specific parameters. Model training used the best-fitting TPM parameters corresponding to the available 2621 reconstructed traces and matching covariates. The model outputs the 5 predicted synapse-specific parameters for any directional pair of neuron types and desired choice of covariates.
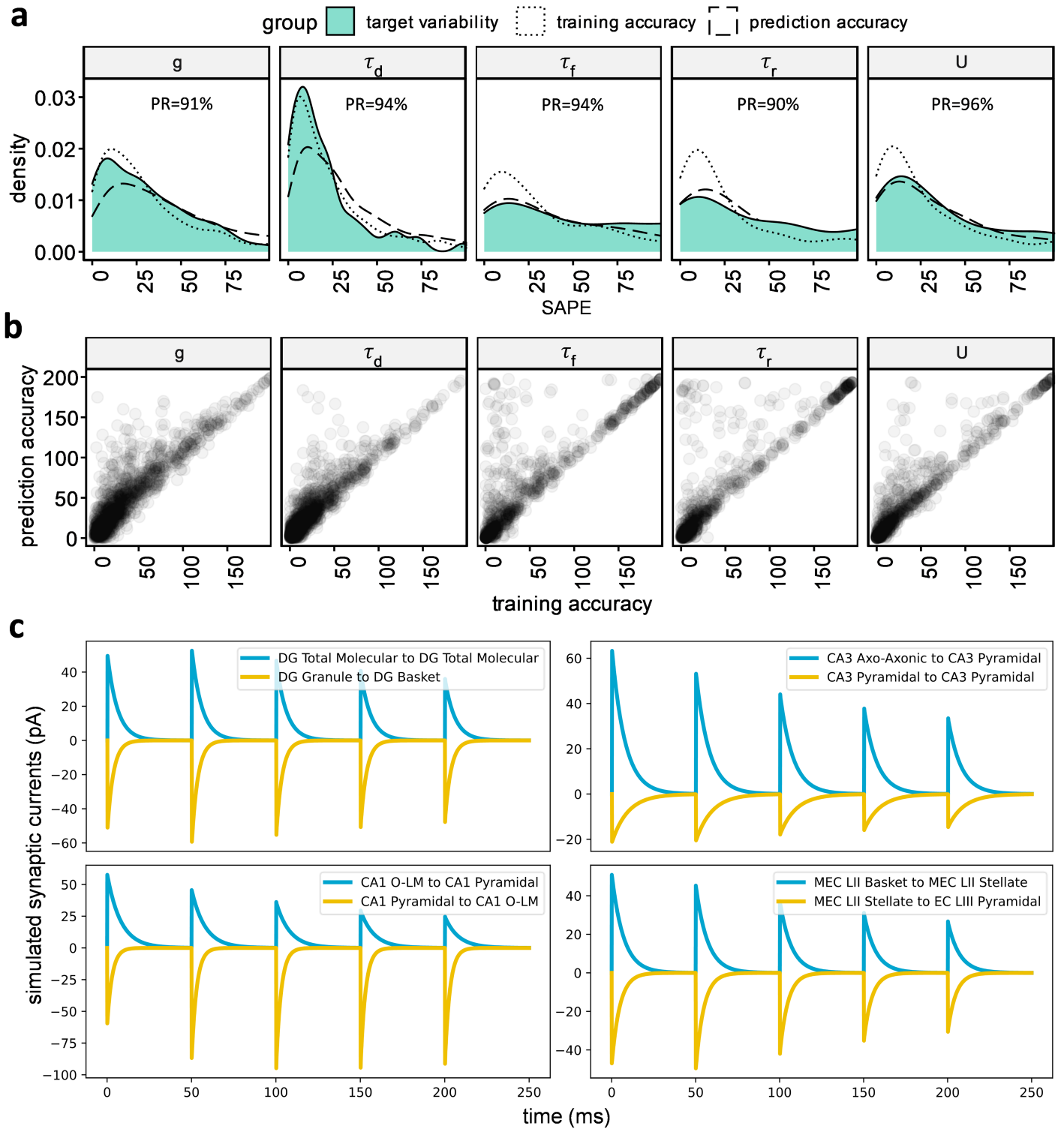
Figure 3

Validation and representative output of the deep learning model for unitary signals. (a) Probability distribution functions of three measures of data mismatch for each of the 5 TPM parameters. Target variability is the distance of a training data point from the average of targets with identical features. This measure of variability in the experimental dataset defines the ideal limit of model accuracy. Training accuracy is the symmetric absolute percentage error (SAPE) of the model output relative to a target on

which it was trained. Prediction accuracy is the SAPE of the model output relative to a target on which it was not trained, using the jackknife (leave-one-out) method. The overall similarity of distributions indicates that the model achieved a level of accuracy comparable to the reproducibility of corresponding experimental data. The prediction reliability (PR) is the proportion of model outputs falling within the 95% confidence interval of the experimental data with identical features. (b) Prediction and training accuracy are highly correlated for all 5 parameters, suggesting the absence of overfitting. (c) Simulated synaptic traces using predicted parameters in standard condition showed a wide range of amplitudes and kinetics as well as different forms of short-term plasticity. Glutamatergic and GABAergic examples are provided for every area involved in the tri-synaptic circuit.

a

Model Parameters: | Conditions: Species: Rat | Sex: Male | Age: P14 | Temperature: 22 Celsius | Recording Mode (-60 mV): Voltage-clamp | Submit: Update

Parameters: g, τ_d, τ_r, τ_f, U

- Digitized/reconstructed traces
- Training data for machine learning
- Normalized/completed synaptic data

Species: Rat / Mouse
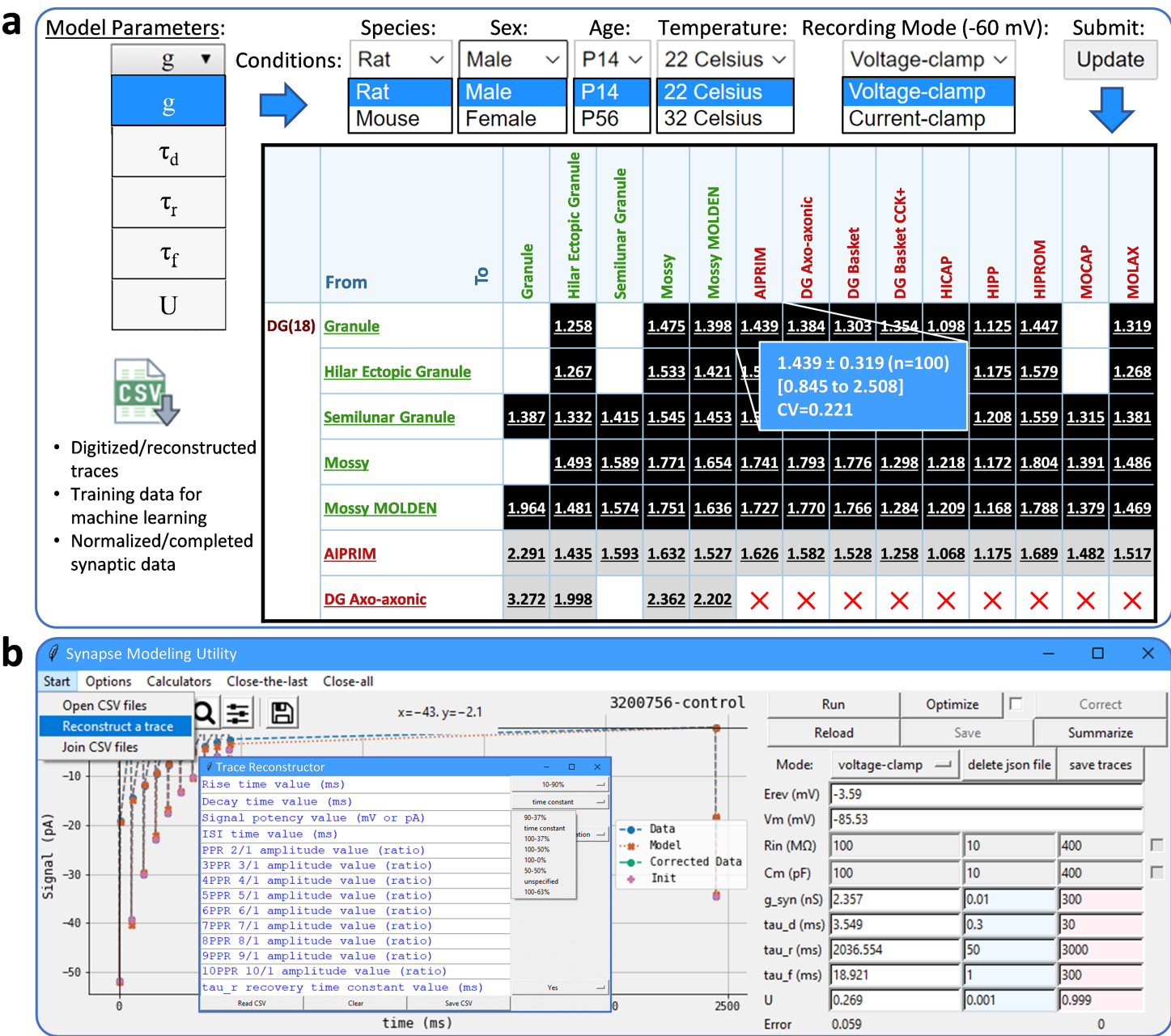Sex: Male / Female
Age: P14 / P56
Temperature: 22 Celsius / 32 Celsius
Recording Mode: Voltage-clamp / Current-clamp

From \ To	Granule	Hilar Ectopic Granule	Semilunar Granule	Mossy	Mossy MOLDEN	AIPRIM	DG Axo-axonic	DG Basket	DG Basket CCK+	HICAP	HIPP	HIPROM	MOCAP	MOLAX
DG(18) Granule		1.258		1.475	1.398	1.439	1.384	1.303	1.354	1.098	1.125	1.447		1.319
Hilar Ectopic Granule		1.267		1.533	1.421	1.5					1.175	1.579		1.268
Semilunar Granule	1.387	1.332	1.415	1.545	1.453	1.5					1.208	1.559	1.315	1.381
Mossy		1.493	1.589	1.771	1.654	1.741	1.793	1.776	1.298	1.218	1.172	1.804	1.391	1.486
Mossy MOLDEN	1.964	1.481	1.574	1.751	1.636	1.727	1.770	1.766	1.284	1.209	1.168	1.788	1.379	1.469
AIPRIM	2.291	1.435	1.593	1.632	1.527	1.626	1.582	1.528	1.258	1.068	1.175	1.689	1.482	1.517
DG Axo-axonic	3.272	1.998		2.362	2.202	✕	✕	✕	✕	✕	✕	✕	✕	✕

1.439 ± 0.319 (n=100)
[0.845 to 2.508]
CV=0.221

b

Synapse Modeling Utility

Start | Options | Calculators | Close-the-last | Close-all

Open CSV files
Reconstruct a trace
Join CSV files

x=-43, y=-2.1   3200756-control

Run | Optimize | Correct
Reload | Save | Summarize

Mode: voltage-clamp | delete json file | save traces

Trace Reconstructor
Rise time value (ms)   10-90%
Decay time value (ms)   time constant
Signal potency value (mV or pA)   90-37%
ISI time value (ms)   100-37%
PPR 2/1 amplitude value (ratio)   100-50%
3PPR 3/1 amplitude value (ratio) 50-50%
4PPR 4/1 amplitude value (ratio) 100-0%
5PPR 5/1 amplitude value (ratio) unspecified
6PPR 6/1 amplitude value (ratio) 100-63%
7PPR 7/1 amplitude value (ratio)
8PPR 8/1 amplitude value (ratio)
9PPR 9/1 amplitude value (ratio)
10PPR 10/1 amplitude value (ratio)
tau_r recovery time constant value (ms)

Read CSV | Clear | Save CSV | Yes

- Data
- Model
- Corrected Data
- Init

Erev (mV) -3.59
Vm (mV)   -85.53
Rin (MΩ)   100   10   400
Cm (pF)   100   10   400
g_syn (nS) 2.357 0.01 300
tau_d (ms) 3.549 0.3   30
tau_r (ms) 2036.554 50 3000
tau_f (ms) 18.921 1   300
U   0.269 0.001 0.999
Error   0.059   0

Signal (pA) axis: -10, -20, -30, -40, -50
time (ms) axis: 0 ... 2500

Figure 4

Comprehensive open access to data and tools. (a) The full set of normalized synaptic data for the entire entorhinal-hippocampal circuit in 32 different conditions (any combination of rat/mouse, male/female, young/adult, body/room temperature, and voltage-/current-clamp), the reconstructed synaptic traces with original references and annotated metadata, and the machine learning training data are all freely available at Hippocampome.org/synapse . For each synaptic parameter of every potential connection, we supply the mean, standard deviation, and range of 100 deep-learning model predictions. (b) Our high-performance synapse modeling tool (Hippocampome.org/SynapseModelingTools) is equipped with a Trace Reconstructor and trace correction algorithm.
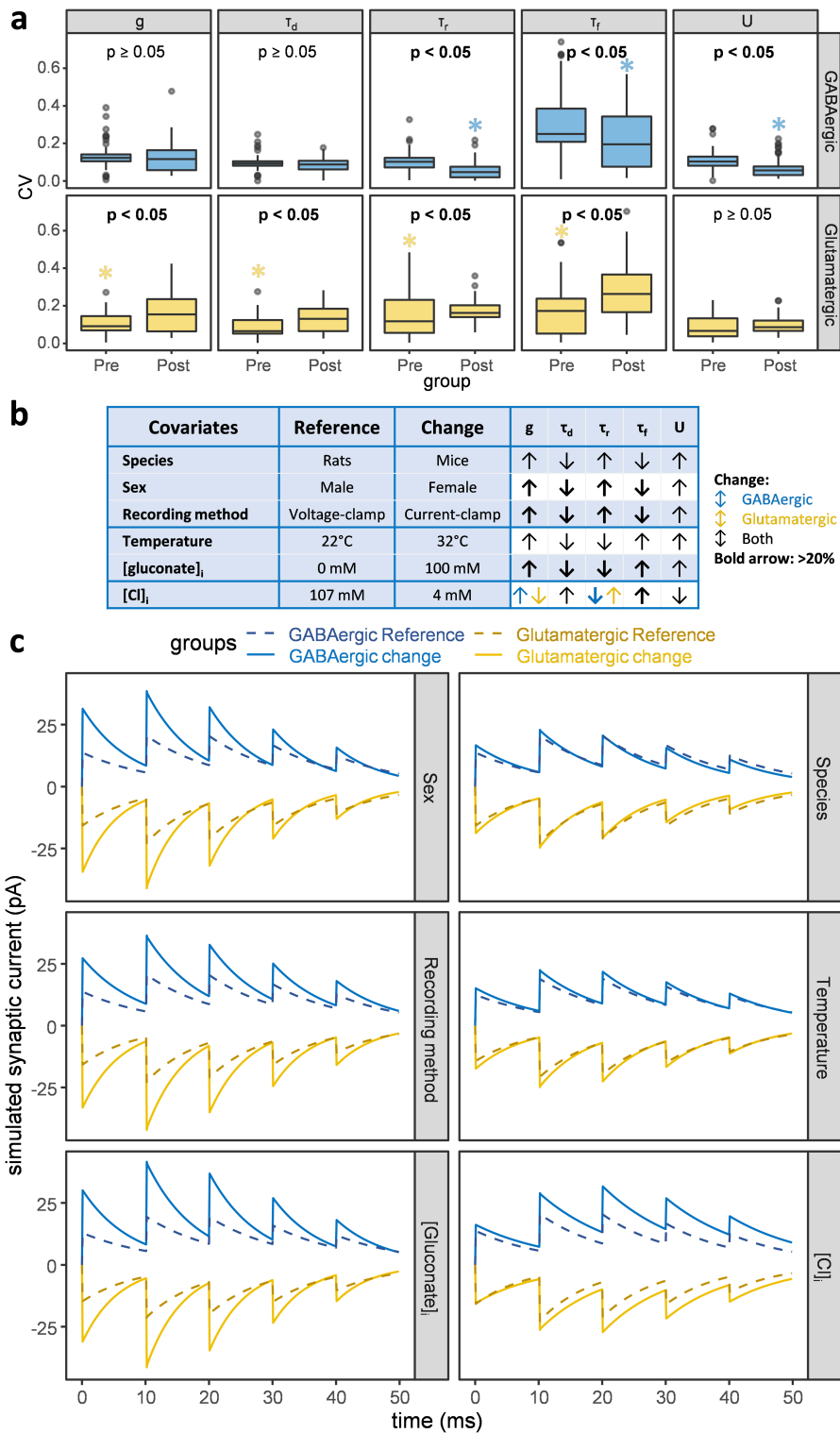
Figure 5

Principal determinants of synaptic properties. (a) To ascertain the relative importance of presynaptic axons and postsynaptic dendrites on synaptic dynamics, we measured the coefficient of variation (CV) of all 5 parameters for each (presynaptic or postsynaptic) neuron type across its potential connections. We then assessed the difference between these two groups by unpaired Wilcoxon test. A significantly lower variability (asterisks) indicates a dominant role of that group in defining the synaptic signal. (b) To

investigate the impact of covariates on synaptic parameters, we changed one experimental condition at a time and assessed the differences by paired Wilcoxon test. All changes were statistically significant; bold arrows indicate differences >20%. (c) To simulate a consensus signal for each group in every pair of conditions, we averaged the 5 synaptic parameters across all relevant (GABAergic or glutamatergic) connections. Comparatively, sex, recording method, and [gluconate]i had the greatest phenomenological impact (in these simulations, Vh=-30 mV, GABAA Erev=-60 mV, and AMPA Erev=0 mV).
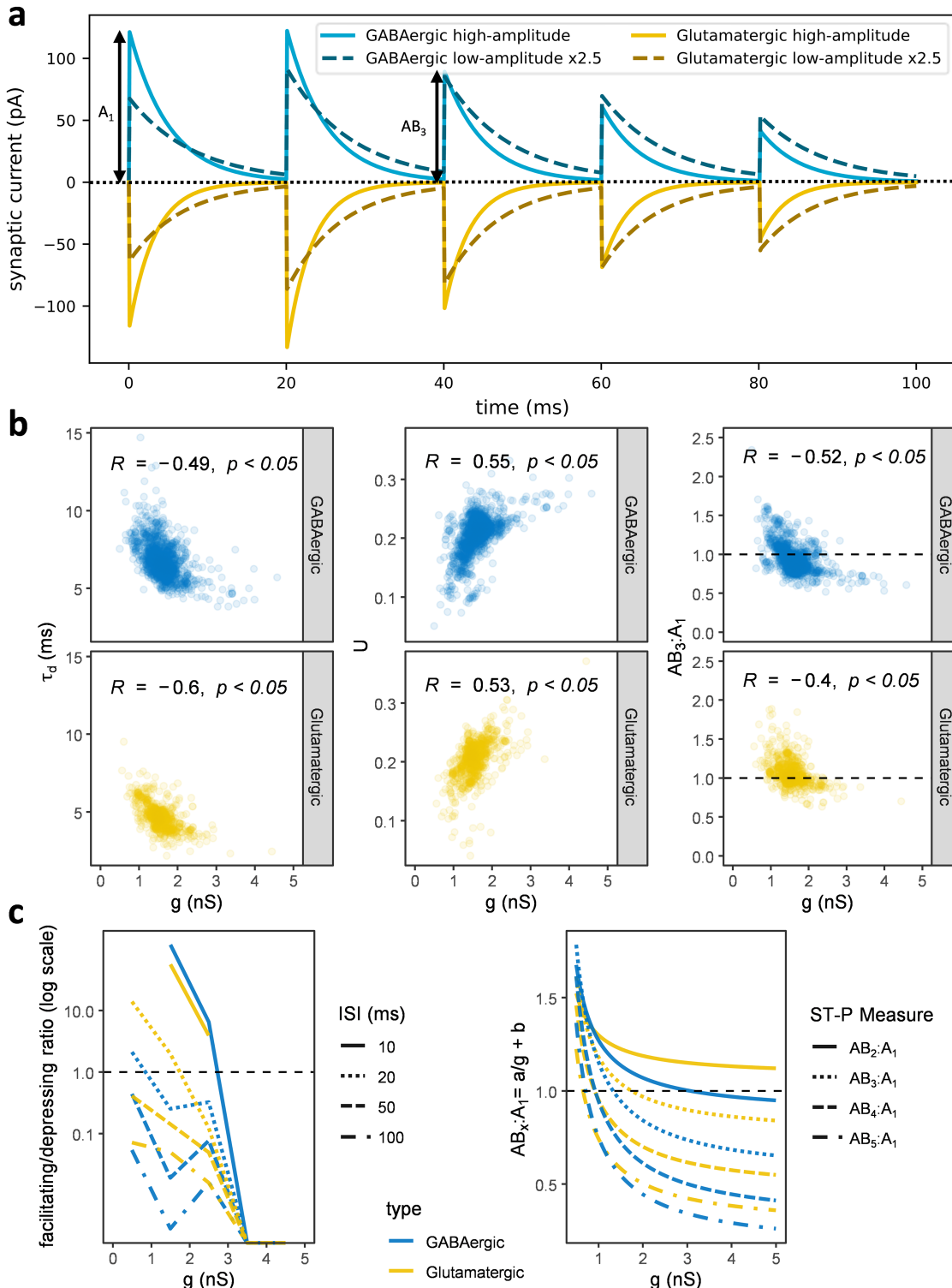

Figure 6

Synaptic conductance entails kinetics and short-term plasticity. (a) We averaged the synaptic parameters of the 30 potential connections with the largest conductance (high-amplitude) and of the 30 with the smallest one (low-amplitude) to compare their simulated consensus signals. The low- and high-amplitude groups exhibited respectively short-term facilitation and depression (ISI=20 ms, Vh=-35 mV, GABAA Erev=-70 mV, and AMPA Erev=0 mV). A1 is the synaptic amplitude of the first event; AB3 is the amplitude from the baseline of the third event. (b) Considering all connections, synaptic amplitude correlates with kinetics and short-term plasticity (ST-P). The negative correlation between g and τd (left) indicates that synapses with large conductance tend to have faster signal decays. The positive correlation between g and U (middle) suggests that high-amplitude synapses have higher resource utilization. The negative correlation between g and the ratio from the baseline of the third event, AB3:A1, (right) shows that high-amplitude synapses depress more. (c) The ratio between facilitation (AB3:A1 > 1) and depression (AB3:A1 ≤ 1) decreases as a function of conductance (left) with a transition from mainly facilitating to mainly depressing between 1 nS (GABAergic) and 1.7 nS (glutamatergic) for 20 ms ISI. Fitting the dependence on g of the ratio from the baseline of the xth event, ABx:A1, with an inverse first-order polynomial function (right) reveals that earlier synaptic events (e.g., AB2:A1) tend to facilitate while later ones (e.g., AB5:A1) tend to depress. The trend from facilitation to depression with increasing conductance is robust to ST-P measure.
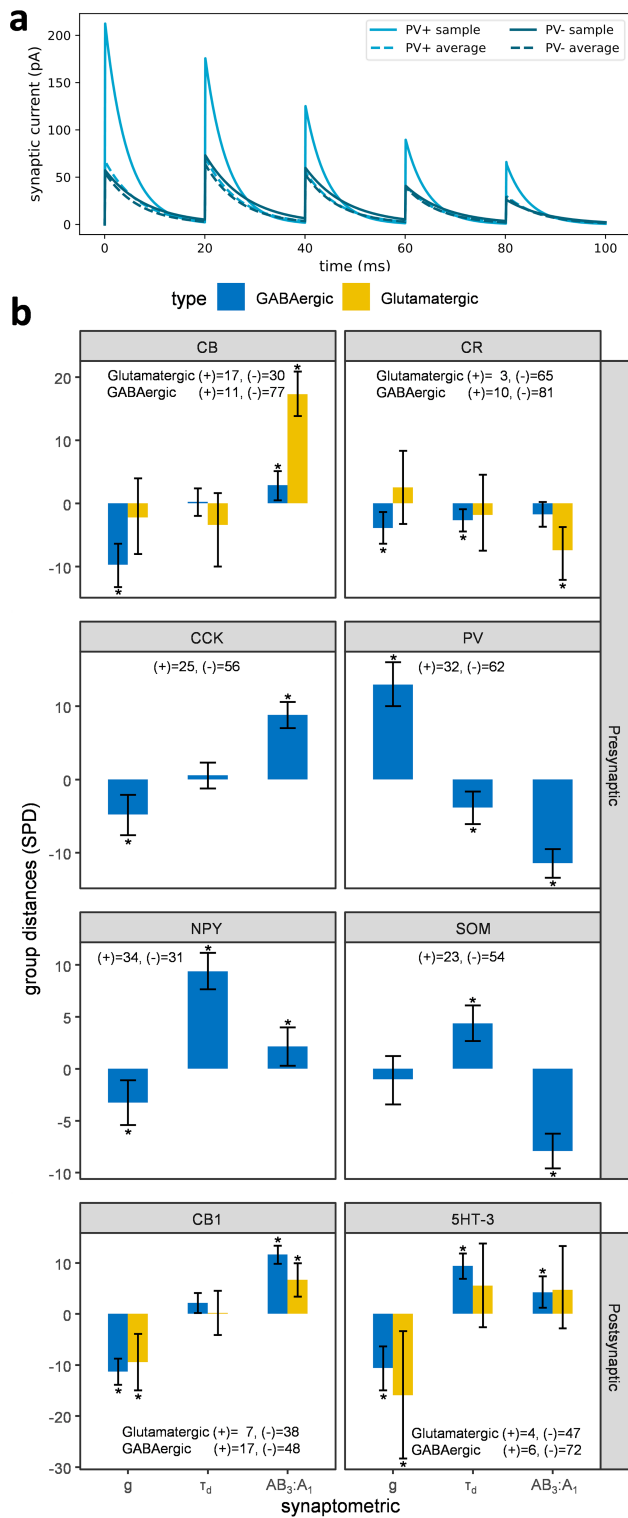
Figure 7

Presynaptic and postsynaptic molecular markers of synaptic physiology. (a) Comparison of synaptic signals between presynaptic neuron types expressing (+) or not expressing (-) parvalbumin (PV). The consensus trace was simulated with synaptic parameters averaged across all potential connections in each group. The sample traces are from the CA1 Basket PV to CA1 Pyramidal connection (+), and from CA1 Basket CCK to CA1 Pyramidal (-). (b) Symmetric percentage differences (SPD) in synaptic

parameters between potential connections grouped by the expression or absence of specific presynaptic or postsynaptic molecular markers (with corresponding samples sizes). Positive values signify that the measurement is larger in the (+) than in the (-) group, and vice versa. Error bars indicate confidence intervals and asterisks denote statistical significance by Wilcoxon test.

Supplementary Files

This is a list of supplementary files associated with this preprint. Click to download.

- Table1.docx
- SupplementaryVideos.mp4
- Fig.S1.tif
- Fig.S2.tif
- Fig.S3.tif
- Fig.S4.tif
- Fig.S5.tif
- Fig.S6.tif
- Fig.S7.tif
- Fig.S8.tif
- Fig.S9.tif
- S.Materials51921gaaNN.docx
- Methods.docx